ADVANCED MATERIALS
www.advmat.de

Thin Films of Magnetically Doped Topological Insulator with Carrier-Independent Long-Range Ferromagnetic Order

Cui-Zu Chang, Jinsong Zhang, Minhao Liu, Zuocheng Zhang, Xiao Feng, Kang Li, Li-Li Wang, Xi Chen, Xi Dai, Zhong Fang, Xiao-Liang Qi, Shou-Cheng Zhang, Yayu Wang, Ke He,* Xu-Cun Ma, and Qi-Kun Xue*

In recent years, topological insulators (TIs), as a class of new concept quantum materials, have received substantial research interests from not only condensed matter physics but also material science.[1,2] A TI has its bulk band gapped at Fermi level, the same as usual insulators, but hosts gapless, Dirac-type, and spin-split surface states at all of its surfaces which are protected by the time reversal symmetry (TRS). The special kind of surface states is expected to exhibit various unique quantum phenomena which may bring revolutionary developments in low power electronics and topological quantum computation.[1,2] A large portion of the quantum phenomena results from breaking of the TRS of TIs by, say, introducing ferromagnetism in them.[3–6] For example, a thin film of a ferromagnetic TI, no matter three-dimensional (3D) or two-dimensional (2D) one, with perpendicular magnetic anisotropy is predicted to show quantum Hall (QH) effect without needing external magnetic field, very high quality of samples, and even low temperature, because the special QH effect does not depend on the formation of well-defined Landau levels.[3–6] This kind of easy access QH effect, known as quantized anomalous Hall (QAH) effect, has been sought after for decades since its realization would open the possibility of applying the novel QH effect into real devices.[7–10]

Doping magnetic impurities is a convenient approach to bring long-range ferromagnetic order in TIs, as demonstrated by the success of diluted magnetic semiconductors (DMSs).[11–13] Ferromagnetism has been realized in several Bi_2Se_3 family

C.-Z. Chang, K. Li, Prof. L.-L. Wang, Prof. X. Dai, Prof. Z. Fang, Prof. K. He, Prof. X.-C. Ma, Prof. Q.-K. Xue
Beijing National Laboratory for Condensed Matter Physics and Institute of Physics
The Chinese Academy of Sciences
Beijing 100190, P. R. China
E-mail: kehe@aphy.iphy.ac.cn

J.-S. Zhang, M.-H. Liu, Z.-C. Zhang, X. Feng, Prof. Y.-Y. Wang, Prof. X. Chen, Prof. Q.-K. Xue
State Key Lab of Low Dimensinal Quantum Physics
Department of Physics
Tsinghua University
Beijing 100084, P. R. China
E-mail: yayuwang@tsinghua.edu.cn
Prof. X.-L. Qi, Prof. S.-C. Zhang
Department of Physics
Stanford University
Stanford, California 94305-4045, USA

DOI: 10.1002/adma.201203493

TIs[14–17] doped with impurities of 3d metals.[18,19] Observation of magnetically induced gap-opening[3,20] in the Dirac surface states, a sign of broken TRS, has been reported.[21,22] However for the realizations of the QAH effect and other novel magnetoelectric phenomena in a magnetically doped TI, a crucial point is that the ferromagnetism should survive the insulating regime, that is, independent of bulk carriers, because Dirac surface states always locate in the bulk gap.[3–6] This requirement rejects the RKKY-type carrier-mediated ferromagnetic coupling dominating conventional DMSs as an applicable mechanism for the ferromagnetism in magnetically doped TIs to show QAH effect. Recently it has been predicted that long-range ferromagnetic coupling free of carriers is possible in magnetically doped Bi_2Se_3 family TIs due to the large van Vleck magnetic susceptibility resulting from their inverted band structures.[5] In this work, in molecular beam epitaxy (MBE) grown thin films of Cr-doped ternary TI material $(Bi_xSb_{1-x})_2Te_3$,[23] the electrochemical potential of which can be efficiently controlled by both Bi:Sb ratio and electrical field effect, we have experimentally realized long-range ferromagnetic order independent of carriers. Furthermore, an unusually large anomalous Hall (AH) effect has been observed in these films when the carrier density is reduced to a very low level, which represents a firm step towards the realization of the QAH effect.

With standard MBE co-evaporation method,[18,24–27] we have prepared Cr-doped $(Bi_xSb_{1-x})_2Te_3$ thin films on several kinds of substrates: sapphire (0001), Si(111), and $SrTiO_3$ (111) substrates, to meet the different requirements of various experiments. During growth, the substrates are kept at a relatively low temperature (~180 °C). This way, higher Cr doping level can be achieved compared to the thermodynamically stable bulk phase.[18] To observe QAH effect in a ferromagnetic TI film, the film thickness should be as thin as possible, to minimize the conduction contribution from side surfaces, on the condition that the gap induced by hybridization between top and bottom surface states[24] is smaller than exchange energy of ferromagnetism (around several meV for the Curie temperature of ~30K of the present samples), to ensure only one pair of spin subbands inverted.[4,5] Therefore we choose 5 QL thick films for the present studies, since the hybridization gap is less than 1 meV at this thickness.[28]

Figure 1a shows a typical scanning tunneling microscope (STM) image of the surface morphology of a 5QL $Cr_{0.22}Sb_{1.78}Te_3$ film. Atomically flat terraces can be observed in large scale without traces of clusters or inhomogeneous regions, which indicates uniform distribution of Cr atoms in Sb_2Te_3 matrix.

 © 2013 WILEY-VCH Verlag GmbH & Co. KGaA, Weinheim

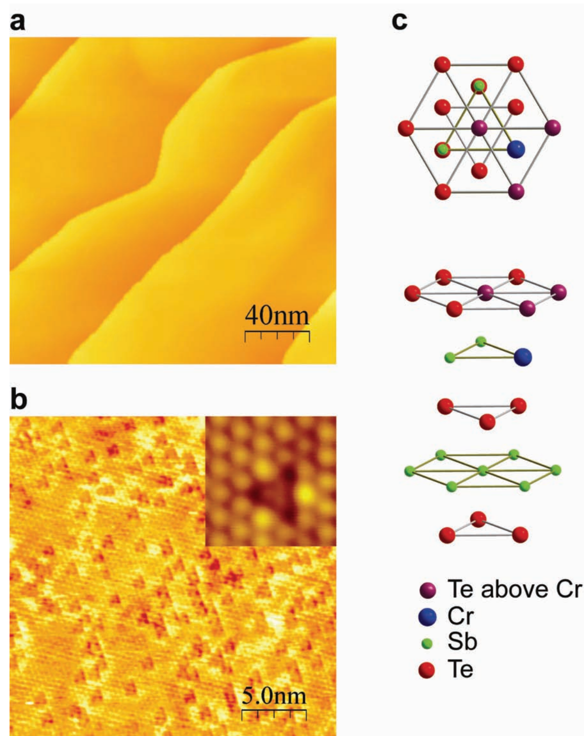

Figure 1. Surface morphology and structure of Cr-doped Sb_2Te_3. a) STM image (100 nm × 100 nm) of the surface morphology of $Cr_{0.22}Sb_{1.78}Te_3$. b) STM image (25 nm × 25 nm) showing Cr impurities in Sb_2Te_3 matrix. The inset displays a high-resolution STM image near a single Cr impurity. c) Atomic structural model indicating the position of a Cr impurity in Sb_2Te_3 lattice.

Cr impurities manifest themselves in STM images as randomly distributed triangle-shaped dark features on the surface, as shown in Figure 1b (a sample with lower Cr doping level is used here to resolve each impurity more clearly.). Each triangle is composed of three dark spots on the positions of topmost Te atoms (see the high-resolution image in the inset of Figure 1b). Since all the triangles point to the same direction, they are unlikely Cr “trimers” but single Cr atoms occupying subsurface Sb sites, reducing the local density of states of the three above Te atoms (see the structural model shown in Figure 1c).[29] Uniform Cr doping is also seen in other $Cr_{0.22}(Bi_xSb_{1-x})_{1.78}Te_3$ films with different Bi contents and confirmed by the structure and composition analyses based on cross-sectional high resolution transmission electronic microscopy (HRTEM) (see Supplementary Information).

Figure 2 displays the band structures near Fermi level of 5QL $Cr_{0.22}(Bi_xSb_{1-x})_{1.78}Te_3$ films with different Bi content (x) measured by angle-resolved photoemission spectroscopy (ARPES) at room temperature. The upper panels (Figures 2a–2d) show the grey scale bandmaps (the 2nd differentiated data are used to highlight the features), and the lower ones (Figures 2e–2h) show the corresponding momentum distribution curves (MDCs) to display the spectra in more detail. Two linearly dispersed bands crossing Fermi level are observed in the spectra for $Cr_{0.22}Sb_{1.78}Te_3$ (Figures 2a and 2e), which have little difference with that of pure Sb_2Te_3 and can be attributed to the Dirac surface bands.[28,31] The Dirac point locates above Fermi level due to p-doping of the sample. Doping Bi has little influence on the Dirac surface bands, but shifts the Fermi level upwards, from below the Dirac point (Figures 2b and 2f for x = 0.1) to near the charge neutral point around x = 0.25 (Figures 2c and 2g), and then to above the Dirac point (Figures 2d and 2h for x = 0.4). It is similar to the observation of p-n crossover in $(Bi_xSb_{1-x})_2Te_3$ without Cr doping,[23] except for shift of the position of charge neutral point to Bi_2Te_3 side, due to extra holes brought by Cr. The variation of carriers from p-type to n-type is mainly caused by the change in the relative density of different types of defects, acceptor or donor, in different chemical environments: in Bi_2Te_3, donor defects (Te on Bi antisite) have lower formation energy and dominate the film,[31] while in Sb_2Te_3, acceptor defects (Sb vacancies and Sb on Te antisite) are energetically favored.[32] The existence of Dirac surface bands in all the samples suggests that the materials are still 3D TIs even at a rather high Cr doping level (>10%), without experiencing any topological phase transition. Magnetically induced gap-opening at Dirac point is not observed, since the TRS still holds in paramagnetic phase at the measurement temperature of ARPES.[3]

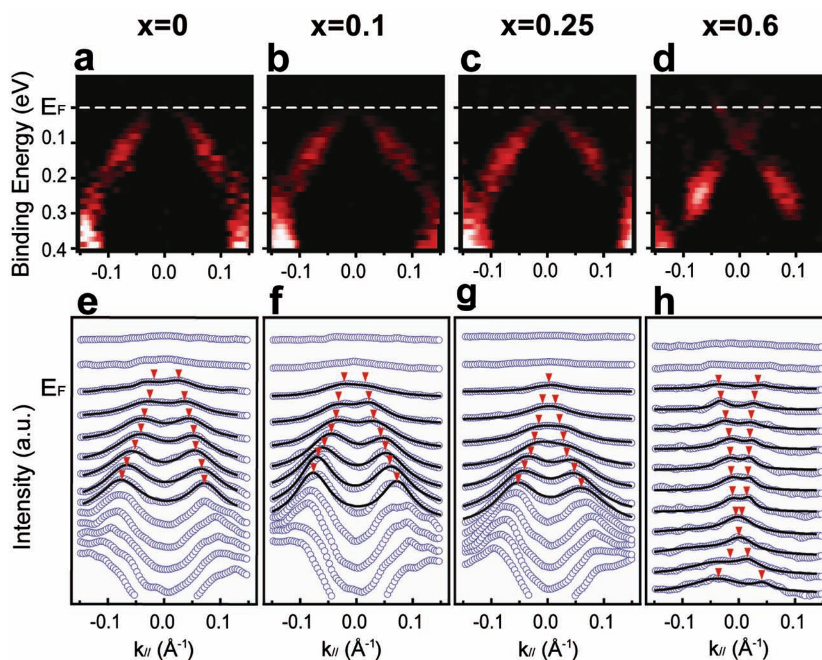

Figure 2. The Dirac surface states of 5QL $Cr_{0.22}(Bi_xSb_{1-x})_{1.78}Te_3$ films measured by ARPES. a–d) ARPES grey-scale bandmaps of $Cr_{0.22}(Bi_xSb_{1-x})_{1.78}Te_3$ films with x = 0 (a), x = 0.1 (b), x = 0.25 (c), and x = 0.6 (d). e–h) ARPES MDCs corresponding to a–d). The blue empty circles are data points; the black solid lines are fitting results with double Lorentz peak; the red triangles indicate the fitted peak positions.

© 2013 WILEY-VCH Verlag GmbH & Co. KGaA, Weinheim

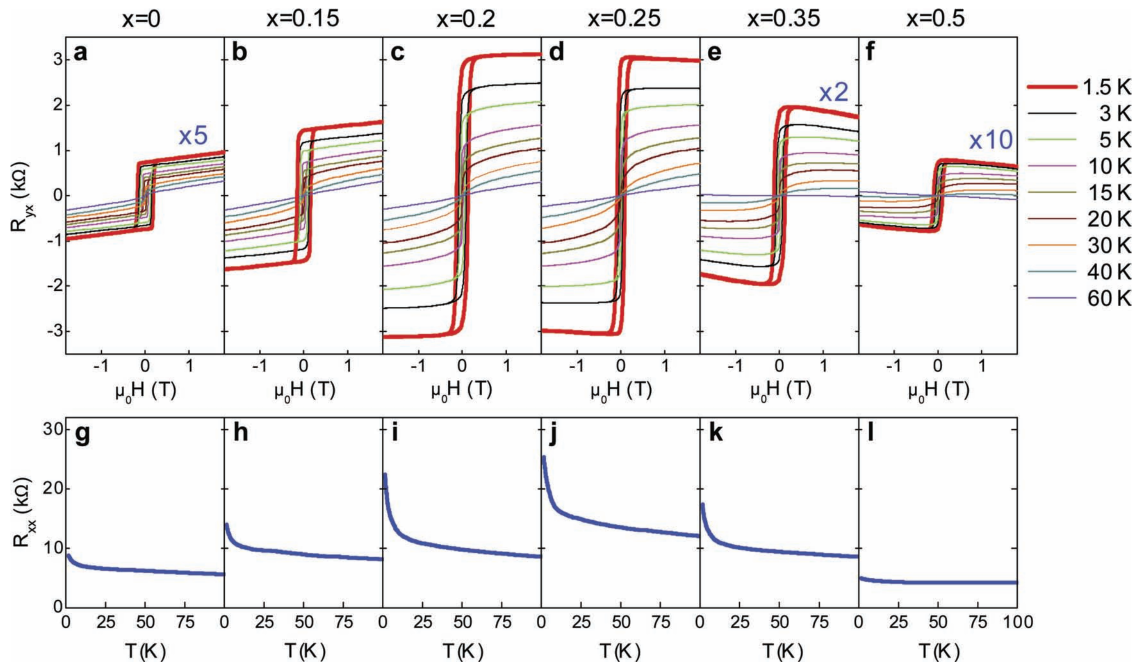

Figure 3. Transport results of 5QL $Cr_{0.22}(Bi_xSb_{1-x})_{1.78}Te_3$ films grown on sapphire (0001). a–f) Magnetic field dependent Hall resistance of the films with x = 0 (a), x = 0.15 (b), x = 0.2 (c), x = 0.25 (d), x = 0.35 (e), and x = 0.5 (f) measured at different temperatures. g–l) Temperature dependent longitudinal resistance R_{xx} of the films with x = 0 (g), x = 0.15 (h), x = 0.2 (i), x = 0.25 (j), x = 0.35 (k), and x = 0.5 (l).

Figure 3 shows the transport measurement data of 5QL $Cr_{0.22}(Bi_xSb_{1-x})_{1.78}Te_3$ films grown on sapphire (0001) substrates with different Bi contents. The upper panels (Figures 3a–3f) display the magnetic field ($\mu_0 H$) dependent Hall resistance (R_{yx}) measured at different temperatures. The lower ones (3g–3l) display the temperature dependent longitudinal resistance (R_{xx}). The total Hall resistance of a magnetic sample is expressed as:[10]

$$R_{yx} = R_0 H + R_{AH}(M) \tag{1}$$

The first term is the ordinary Hall (OH) resistance (R_{OH}) responsible for the linear R_{yx} at high field with the slope R_0, known as Hall coefficient, determined by the type and density of carriers of the sample. The second term is the AH resistance (R_{AH}), reflecting the magnetization reversal of the sample at low field (below the saturation field).[10] For all the films, the R_{yx}-$\mu_0 H$ curves measured at 1.5 K (the thicker ones in Figures 3a–3f) show nearly square-shaped hysteresis loops at low field, suggesting good long-range ferromagnetic order with the easy magnetization axis perpendicular to the sample plane. Meanwhile with the increasing Bi content (x), the slope of the linear background at high field evolves from positive to negative, indicating the change of the dominating carriers from p- to n-type at around x = 0.2 ~ 0.25, consistent with the above ARPES observations. The temperature dependent R_{xx} curves of all the films (Figures 3g–3l) exhibit a typical insulating behavior. Among them the samples with x = 0.2 and 0.25 show the largest values, both exceeding 20 kΩ at 1.5K, which can be attributed to their low carrier densities near p-n crossover region. So we can see that the ferromagnetism of Cr-doped $(Bi_xSb_{1-x})_2Te_3$ always holds despite of the significant change in carrier density and type induced by different Bi concentrations. The ferromagnetism has also been confirmed by direct magnetization measurements with SQUID magnetometer (see Supplementary Information), which shows similar hysteresis loops with those of AH effect. The magnetic moment per Cr ion, estimated from the SQUID data, is ~3 μ_B, which is basically that of a Cr^{3+} ion and varies little with Bi content. The moment value is quite reasonable since 3+ is the most stable oxidation state of Cr and the above STM result have demonstrated Cr substitution for Sb^{3+} ions.

We can estimate the Curie temperatures (T_Cs) of the $Cr_{0.22}(Bi_xSb_{1-x})_{1.78}Te_3$ films through temperature dependent R_{AH}, which is defined as R_{yx} at zero field[10] and reflects the spontaneous magnetization of the samples. **Figure 4**a plots the T_Cs of the samples of different Bi contents. The corresponding carrier densities estimated by OH effect are shown as the tick labels of the top axis. It is to note that the carrier density values can only be treated semi-quantitatively, especially near the charge neutral point, because the slope of OH effect can be influenced by AH effect and magnetoresistance (MR).[33] From Figure 4a, one can see that T_C experiences little variation with carrier density and type, always around 30K~35K, even in the rather insulating samples around p-n crossover region (blue area), which clearly indicates carrier independence of the ferromagnetism.

The AH effect, on the other hand, exhibits a dramatic and systematic change with Bi doping. R_{AH} is only 148 Ω at 1.5 K for x = 0 (note that the data shown in Figure 3a are multiplied by 5), but abruptly increases to 1.4 kΩ, about one order of magnitude larger for x = 0.15. The value is further enhanced to 2.8 kΩ at x = 0.2, and 2.9 kΩ at x = 0.25, respectively. But as x reaches 0.35, R_{AH} rapidly drops to 900 Ω, and then to only 72 Ω at x = 0.5. The evolution of R_{AH} with Bi content and carrier density

 © 2013 WILEY-VCH Verlag GmbH & Co. KGaA, Weinheim

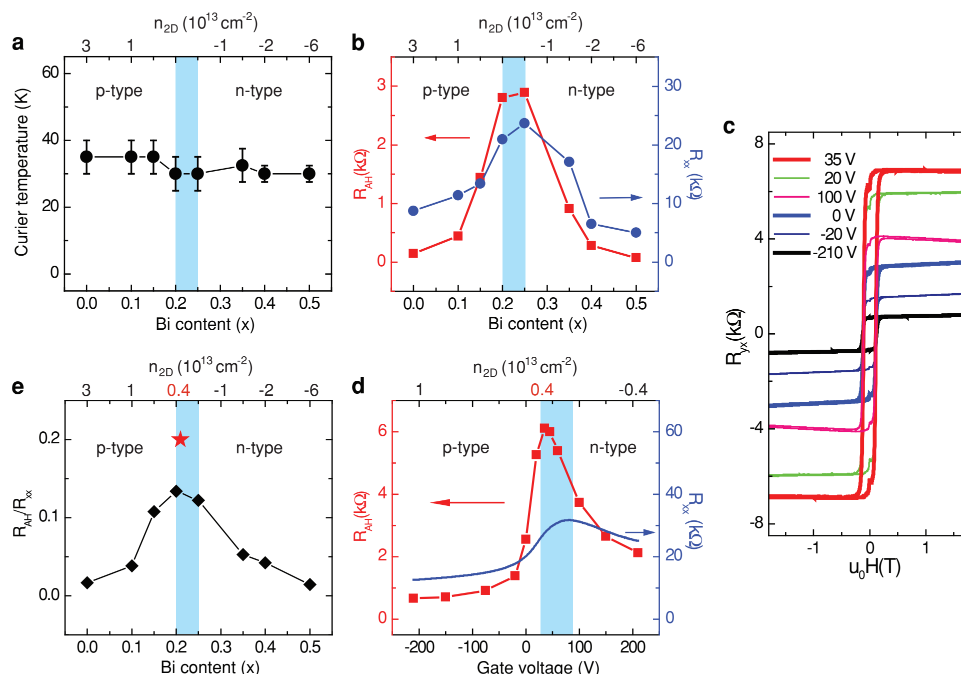

Figure 4. Ferromagnetism and AH effect of $Cr_{0.22}(Bi_xSb_{1-x})_{1.78}Te_3$ films at different carrier density and type. a) Dependence of Curie temperature (T_C) on Bi content (x) (bottom axis) and carrier density (top axis). Error bars represent the temperature spacing in R_{AH}-T measurements. b) Dependence of AH resistance (R_{AH}) (red solid squares) and longitudinal resistance (R_{xx}) (blue solid circles) at 1.5 K on Bi content (x) (bottom axis) and carrier density (top axis). c) Magnetic field dependent Hall resistance R_{yx} of a 5QL $Cr_{0.22}(Bi_{0.2}Sb_{0.8})_{1.78}Te_3$ film grown on $SrTiO_3$ (111) at different back-gate voltages measured at 250 mK. d) Dependence of R_{AH} (red solid squares) and R_{xx} (blue solid line) of the 5QL $Cr_{0.22}(Bi_{0.2}Sb_{0.8})_{1.78}Te_3$ film grown on $SrTiO_3$(111) substrate on back-gate voltages at 250 mK. e) Dependence of R_{AH}/R_{xx} on Bi content (x) (bottom axis) and carrier density (top axis). Black solid diamonds represent the data obtained from Figure 4b. The red star represents the value obtained from a Hall measurement at 250 mK, 15 Tesla on the $Cr_{0.22}(Bi_{0.2}Sb_{0.8})_{1.78}Te_3$ film grown on $SrTiO_3$ (111) with back-gate voltage 35 V. The blue areas in a, b, d, and e indicate the approximate p-n crossover regions.

is summarized in Figure 4b. A maximum occurs near the p-n crossover region (blue area), with R_{AH} about 40 times larger than the minimum value. Evolution of R_{xx} with Bi content is also plotted here, exhibiting a similar maximum with R_{AH}, but with smaller relative variation than that of R_{AH}. Figure 4e displays the R_{AH}/R_{xx} ratio, i.e. tangent of the AH angle, for different Bi contents (black solid diamonds). The ratio is only about 0.02 for high carrier density samples but increases by more than 5 times near the crossover region.

To further demonstrate the dependence of ferromagnetism and AH effect on carriers, we have studied the transport properties of the films under the electrical field effect. $SrTiO_3$ (111) is applied as the substrate whose huge dielectric constant at low temperature can be utilized to realize carrier density variation of ~3 × 10^{13}cm^{-2} with back-gate voltage (V_g) between ±210 V for typical substrate thickness of 0.5mm.[34] Figure 4c shows the AH hysteresis loops of a 5QL $Cr_{0.22}(Bi_{0.2}Sb_{0.8})_{1.78}Te_3$ film grown on $SrTiO_3$ (111) measured at 250 mK with different V_gs. R_{AH} changes dramatically with V_g, from 660 Ω at –210 V to 6.1 kΩ (the maximum) at 35 V, as summarized in Figure 4d. R_{xx} also exhibits a peak of ~30 kΩ at 80 V. The R_{AH}/R_{xx} ratio corresponding to R_{AH} = 6.1 kΩ is ~ 0.2 (the red star shown in Figure 4e), indicating an unusually large AH effect.[10] Meanwhile the coercivity and the shape of the hysteresis loops are nearly unchanged with V_g, suggesting little variation in the ferromagnetism. The sheet carrier density around R_{AH} = 6.1 kΩ, determined by the slope of OH effect measured with a magnetic field up to 15 Tesla that is high enough to saturate AH resistance and MR, is ~4 × 10^{12} cm^{-2}. So the field effect experiment also demonstrates the carrier independent ferromagnetism and the greatly enhanced AH effect with the decreasing carrier density.

In most magnetically doped semiconductors/insulators the ferromagnetic coupling is mediated by itinerant carriers through the RKKY-type mechanism; thus the ferromagnetism in these materials is very sensitive to the variation in the density and type of bulk carriers.[11–13] The magnetic TI studied here however shows a robust ferromagnetism with nearly constant Curie temperature in both n- and p-doped regimes and also in the very insulating crossover region in between. The lowest n_{2D} accurately estimated with OH effect is ~4 × 10^{12} cm^{-2}, corresponding to a bulk carrier density of 8 × 10^{18} cm^{-3}, which is too low a carrier density level to form RKKY-type ferromagnetic coupling.[13] Magnetic clusters can contribute to ferromagnetism independent of the carriers. However this possibility can be safely ruled out by the above experimental results: the uniform crystalline structure and homogeneous Cr distribution revealed by STM and HRTEM, the similar magnetic properties obtained by magnetic and transport measurements, and the large average magnetic moment of Cr ion (~3m_B) which is well consistent with the STM observation of random Cr substitution for Sb/Bi^{3+} ions. Furthermore, the AH resistance of Cr-doped $(Bi_xSb_{1-x})_2Te_3$ can reach an unusually large value close to the

© 2013 WILEY-VCH Verlag GmbH & Co. KGaA, Weinheim

order of QH resistance (h/e^2). Although magnetic clusters can also lead to AH effect in the matrix material through "extrinsic" mechanism like skew scattering and side jump,[10] such extrinsic AH effect cannot contribute to so strong AH resistance near QH regime.[36,37] The skew scattering and side-jump mechanisms can be further excluded by the observations of quadratic relation between R_{AH} and R_{xx} (see Supplementary Information) and enhanced R_{AH} with decreasing carrier density.[10]

The doping independent ferromagnetism can be explained naturally by a novel mechanism unique to the magnetically doped 3D TIs. The bulk band structure of the TIs is inverted by the strong spin-orbit coupling so that the valence and conduction bands near Fermi level have similar component (p_z).[14] As discussed theoretically,[5] this unique band structure contributes to the large matrix element of spin operator, and thus leads to a large magnetic susceptibility of valence electrons through the van Vleck mechanism even when the Fermi level lies in the gap. Hence, the spins from different magnetic impurities can be coupled through the large magnetic susceptibility of the valence electrons without needing itinerant carriers. The van Vleck mechanism will lead to linear relationship between Curie temperature and concentration of magnetic impurities,[5] which has been observed in our samples (see Supplementary Information) as well as in Cr-doped Sb_2Te_3 in a previous study.[18] So the carrier-independent ferromagnetism observed in Cr-doped $(Bi_xSb_{1-x})_2Te_3$ is very likely contributed by the van Vleck mechanism.

The thin films of magnetic TIs with insulating ferromagnetism are expected to show the QAH effect if the Fermi level is tuned into the magnetically induced gap opened at the Dirac point.[3–6] The rapidly increasing R_{AH} with the decreasing carrier density is in accord with the theoretically predicted tendency of AH effect approaching the QH plateau.[5,6] The maximum R_{AH} obtained in this work has reached 6.1 kΩ, nearly one fourth of the QH resistance. The corresponding bulk AH resistivity (ρ_{AH}) is about 3 mΩ·cm, among the largest ρ_{AH} ever reported. Furthermore, the tangent of AH angle R_{AH}/R_{xx} also grows rapidly with the depletion of bulk carriers, to an unusually large value of 0.2 in the bulk insulating regime, which is an order of magnitude larger than that of most ferromagnetic materials.[10] In the QAH regime the ratio should be infinite, just like in conventional QH effect, due to the dissipationless QAH edge states. Although so far samples still show a rather large longitudinal resistance, implying that bulk carriers still significantly contribute to the transport result, the greatly enhanced R_{AH}/R_{xx} with the reduced carrier density suggests that the influence from the QAH edge states is becoming more and more important. As far as the current data have shown, R_{AH} and R_{AH}/R_{xx} still keep growing with the decreasing carrier density. The failure of R_{AH} to reach QH plateau should be mainly due to the remaining bulk carriers not completely depleted yet (see Supplementary Information for the discussion). Inhomogeneous chemical potential distribution, band bending, and impurities of the films all can contribute to the bulk carriers. By optimizing the film thickness, growth parameters, and fabricating the films into devices of micrometer or sub-micrometer size with dual-gate structure, it is promising to further reduce the bulk carrier density of the films to reach the QAH regime.

In summary, we have observed robust ferromagnetism in thin films of Cr-doped 3D TI $(Bi_xSb_{1-x})_2Te_3$ against the variation in both carrier density and type, suggesting that the van Vleck mechanism due to the valence electrons with inverted band structure is responsible for the ferromagnetism. The AH resistance reaches an unusually large value of one quarter of QH resistance as the carriers are depleted by doping or gating, manifesting the system as a promising one for realizing the QAH effect and other TI-based magnetoelectric phenomena. The realization of ferromagnetism in samples of both p- and n-doped and in different doping levels also provides a new platform for spintronic applications.

Note added: During peer review of our paper we became aware of related work by Joseph G. Checkelsky et al.[37]

Experimental Section

MBE growth and measurements of STM and ARPES were carried out in one UHV system with the base pressure ~1×10^{-10} mbar. The Cr-doped $(Bi_xSb_{1-x})_2Te_3$ films were grown by co-evaporating Bi (99.9999%), Sb (99.9999%), Cr (99.999%), and Te (99.9999%) from standard Knudsen cells to commercial sapphire (0001), Si(111), or $SrTiO_3$ (111) substrates. The growth was kept in Te-rich condition with the substrate temperature set at ~180 °C. The thicknesses and the compositions of the films are determined by growth time and the fluxes of Cr, Bi, and Sb sources. The fluxes of Sb and Bi are calibrated by the growth rates of Sb_2Te_3 and Bi_2Te_3 thin films, through RHEED oscillation or quantum-well state peak positions in ARPES, respectively. The flux of Cr is calibrated by the atomic percentage in Cr-doped $(Sb_{1-x}Bi_x)_2Te_3$ samples measured with inductively coupled plasma - atomic emission spectra (IRIS Intrepid II, Thermo Scientific). The typical growth rate is about 0.125 QL/minute. In ARPES measurements, photoelectrons are excited by unpolarized He-Iα light (21.21 eV) generated by a Gammadata VUV 5000 helium discharging lamp and collected by a Scienta SES-2002 analyzer. A 20 nm-thick amorphous and insulating Te capping layer was deposited on the top of each film before it is taken out of the UHV chamber for transport measurements. Transport properties are measured in the Hall bar geometry with ac lock-in method.

Supporting Information

Supporting Information is available from the Wiley Online Library or from the author.

Acknowledgements

We would like to thank J. Chen and Y.-Q. Li from Institute of Physics, Chinese Academy of Sciences for their advices on cleaning of $SrTiO_3$ substrates, and thank Y. Wu, X.-L Dong, and Y. Yao from Institute of Physics, Chinese Academy of Sciences and L.-H. Wang and X.-D. Han from Beijing University of Technology for their helps in magnetic and HRTEM characterizations of our samples. This work was financially supported by NBRP of China (Grant Nos. 2012CB921302 and 2009CB929400), NSFC (Grant Nos. 10974237 and 91021006), and the Knowledge Innovation Program of Chinese Academy of Sciences.

Received: August 22, 2012
Revised: October 10, 2012
Published online: January 18, 2013

© 2013 WILEY-VCH Verlag GmbH & Co. KGaA, Weinheim

[1] M. Z. Hasan, C. L. Kane, *Rev. Mod. Phys.* **2010**, *82*, 3045.
[2] X.-L. Qi, S.-C. Zhang, *Rev. Mod. Phys.* **2011**, *83*, 1057.
[3] X.-L. Qi, T. L. Hughes, S.-C. Zhang, *Phys. Rev. B* **2008**, *78*, 195424.
[4] C.-X. Liu, X.-L. Qi, X. Dai, Z. Fang, S.-C. Zhang, *Phys. Rev. Lett.* **2008**, *101*, 146802.
[5] R. Yu, W. Zhang, H. J. Zhang, S.-C. Zhang, X. Dai, Z. Fang, *Science* **2010**, *329*, 61.
[6] K. Nomura, N. Nagaosa, *Phys. Rev. Lett.* **2011**, *106*, 166802.
[7] F. D. M. Haldane, *Phys. Rev. Lett.* **1988**, *61*, 2015.
[8] M. Onoda, N. Nagaosa, *Phys. Rev. Lett.* **2003**, *90*, 206610.
[9] W. K. Tse, Z. Qiao, Y. Yao, A. H. MacDonald, Q. Niu, *Phys. Rev. B* **2011**, *83*, 155447.
[10] N. Nagaosa, J. Sinova, S. Onoda, A. H. MacDonald, N. P. Ong, *Rev. Mod. Phys.* **2010**, *82*, 1539.
[11] H. Ohno, *Science* **1998**, *281*, 951.
[12] T. Dietl, *Nat. Mater.* **2010**, *9*, 965.
[13] T. Dietl, H. Ohno, F. Matsukura, J. Cibert, D. Ferrand, *Science* **2000**, *287*, 1019.
[14] H. J. Zhang, C.-X. Liu, X.-L. Qi, X. Dai, Z. Fang, S.-C. Zhang, *Nat. Phys.* **2009**, *5*, 438.
[15] Y. Xia, D. Qian, D. Hsieh, L. Wray, A. Pal, H. Lin, A. Bansil, D. Grauer, Y. S. Hor, R. J. Cava, M. Z. Hasan, *Nat. Phys.* **2009**, *5*, 398.
[16] D. Hsieh, Y. Xia, D. Qian, L. Wray, J. H. Dil, F. Meier, J. Osterwalder, L. Patthey, J. G. Checkelsky, N. P. Ong, A. V. Fedorov, H. Lin, A. Bansil, D. Grauer, Y. S. Hor, R. J. Cava, M. Z. Hasan, *Nature* **2009**, *460*, 1101.
[17] Y. L. Chen, J. G. Analytis, J.-H. Chu, Z. K. Liu, S.-K. Mo, X.-L. Qi, H. J. Zhang, D. H. Lu, X. Dai, Z. Fang, S.-C. Zhang, I. R. Fisher, Z. Hussain, Z.-X. Shen, *Science* **2009**, *325*, 178.
[18] Y. J. Chien, *Ph.D. thesis, University of Michigan*, **2007**. (http://deep-blue.lib.umich.edu/handle/2027.42/57593)
[19] Y. S. Hor, P. Roushan, H. Beidenkopf, J. Seo, D. Qu, J. G. Checkelsky, L. A. Wray, D. Hsieh, Y. Xia, S.-Y. Xu, D. Qian, M. Z. Hasan, N. P. Ong, A. Yazdani, R. J. Cava, *Phys. Rev. B* **2010**, *81*, 195203.
[20] Q. Liu, C. X. Liu, C. Xu, X.-L. Qi, S.-C. Zhang, *Phys. Rev. Lett.* **2009**, *102*, 156603.
[21] Y. L. Chen, J.H. Chu, J.G. Analytis, Z. K. Liu, K. Igarashi, H.-H. Kuo, X. L. Qi, S. K. Mo, R. G. Moore, D. H. Lu, M. Hashimoto, T. Sasagawa, S.-C. Zhang, I. R. Fisher, Z. Hussain, Z. X. Shen, *Science* **2010**, *329*, 659.
[22] L. A. Wray, S. Y. Xu, Y. Q. Xia, D. Hsieh, A. V. Fedorov, Y. S. Hor, R. J. Cava, A. Bansil, H. Lin, M. Z. Hasan, *Nat. Phys.* **2011**, *7*, 32.
[23] J. Zhang, C. Z. Chang, Z. C. Zhang, J. Wen, X. Feng, K. Li, M. Liu, K. He, L.-L. Wang, X. Chen, Q. K. Xue, X. Ma, Y. Wang, *Nat. Commun.* **2011**, *2*, 574.
[24] Y. Zhang, K. He, C.-Z. Chang, C.-L. Song, L.-L. Wang, X. Chen, J.-F. Jia, Z. Fang, X. Dai, W.-Y. Shan, S.-Q. Shen, Q. Niu, X.-L. Qi, S.-C. Zhang, X.-C. Ma, Q.-K. Xue, *Nature Phys.* **2010**, *6*, 584.
[25] X. Chen, X. C. Ma, K. He, J.-F. Jia, Q.-K. Xue, *Adv. Mater.* **2010**, *23*, 1162.
[26] Y.-Y. Li, G. Wang, X.-G. Zhu, M.-H. Liu, C. Ye, X. Chen, Y. Wang, K. He, L.-L. Wang, X.-C. Ma, H.-J. Zhang, X. Dai, Z. Fang, X.-C. Xie, Y. Liu, X.-L. Qi, J.-F. Jia, S.-C. Zhang, Q.-K. Xue, *Adv. Mater.* **2010**, *22*, 4002.
[27] G. Wang, X. Zhu, J. Wen, X. Chen, K. He, L. L. Wang, X. C. Ma, Y. Liu, X. Dai, Z. Fang, J.-F. Jia, Q.-K. Xue, *Nano Res.* **2010**, *3*, 874.
[28] Y. P. Jiang, Y. L. Wang, M. Chen, Z. Li, C. Z. Song, K. He, L.-L. Wang, X. Chen, X.-C. Ma, Q. K. Xue, *Phys. Rev. Lett.* **2012**, *108*, 016401.
[29] T. Zhang, P. Cheng, X. Chen, J.-F. Jia, X. C. Ma, K. He, L. L. Wang, H. J. Zhang, X. Dai, Z. Fang, X.-C. Xie, Q.-K. Xue, *Phys. Rev. Lett.* **2009**, *103*, 266803.
[30] D. Hsieh, A. V. Fedorov, Y. S. Hor, R. J. Cava, A. Bansil, H. Lin, M. Z. Hasan, *Phys. Rev. Lett.* **2009**, *103*, 146401.
[31] G. Wang, X.-G. Zhu, Y.-Y. Sun, Y.-Y. Li, T. Zhang, J. Wen, X. Chen, K. He, L.-L. Wang, X.-C. Ma, J.-F. Jia, S. B. Zhang, Q.-K. Xue, *Adv. Mater.* **2011**, *2*, 2929.
[32] Y. P. Jiang, Y. Y. Sun, M. Chen, Y. L. Wang, Z. Li, C. L. Song, K. He, L. L. Wang, X. Chen, Q. K. Xue, X. C. Ma, S. B. Zhang, *Phys. Rev. Lett.* **2012**, *108*, 066809.
[33] H. J. Ohno, *Magn. Magn. Mater.* **1999**, *200*, 110.
[34] J. Chen, H. J. Qin, F. Yang, J. Liu, T. Guan, F. M. Qu, G. H. Zhang, J. R. Shi, X.-C. Xie, C. L. Yang, K. H. Wu, Y. Q. Li, L. Lu, *Phys. Rev. Lett.* **2010**, *105*, 176602.
[35] S. B. Ogale, *Adv. Mater.* **2010**, *22*, 3125.
[36] D. Culcer, *Phys. Rev. B* **2011**, *83*, 245441.
[37] J. G. Checkelsky, J. Ye, Y. Onose, Y. Iwasa, Y. Tokura, *Nature Phys.* **2012**, *8*, 729.

© 2013 WILEY-VCH Verlag GmbH & Co. KGaA, Weinheim